International Journal of Astrobiology 9 (4): 265–271 (2010)
doi:10.1017/S1473550410000285

Hubble Space Telescope observations of Europa in and out of eclipse

W.B. Sparks[1], M. McGrath[2], K. Hand[3], H.C. Ford[4], P. Geissler[5], J.H. Hough[6], E.L. Turner[7,8], C.F. Chyba[7], R. Carlson[3] and M. Turnbull[9]

[1]*Space Telescope Science Institute, 3700 San Martin Drive, Baltimore, MD 21218, USA*
e-mail: sparks@stsci.edu
[2]*NASA Marshall Space Flight Center, Huntsville, AL 35812, USA*
[3]*Jet Propulsion Laboratory, California Institute of Technology, MS 183-601, 4800 Oak Grove Drive, Pasadena, CA 91109, USA*
[4]*Department of Physics & Astronomy, The Johns Hopkins University, Bloomberg Center, 3400 N. Charles Street, Baltimore, MD 21218, USA*
[5]*Center for Astrogeology, U.S. Geological Survey, 2255 N. Gemini Drive, Flagstaff, AZ 86001, USA*
[6]*Centre for Astrophysics Research, Science & Technology Research Institute, University of Hertfordshire, College Lane, Hatfield, AL10 9AB, UK*
[7]*Department of Astrophysical Sciences, 122 Peyton Hall, Princeton University, Princeton, NJ 08544, USA*
[8]*The University of Tokyo, Japan*
[9]*Global Science Institute, P.O. Box 252, Antigo, WI 54409, USA*

Abstract: Europa is a prime target for astrobiology and has been prioritized as the next target for a National Aeronautics and Space Administration flagship mission. It is important, therefore, that we advance our understanding of Europa, its ocean and physical environment as much as possible. Here, we describe observations of Europa obtained during its orbital eclipse by Jupiter using the Hubble Space Telescope. We obtained Advanced Camera for Surveys Solar Blind Channel far ultraviolet low-resolution spectra that show oxygen line emission both in and out of eclipse. We also used the Wide-Field and Planetary Camera-2 and searched for broad-band optical emission from fluorescence of the surface material, arising from the very high level of incident energetic particle radiation on ices and potentially organic substances. The high-energy particle radiation at the surface of Europa is extremely intense and is responsible for the production of a tenuous oxygen atmosphere and associated FUV line emission. Approximately 50% of the oxygen emission lasts at least a few hours into the eclipse. We discuss the detection limits of the optical emission, which allow us to estimate the fraction of incident energy reradiated at optical wavelengths, through electron-excited emission, Cherenkov radiation in the ice and fluorescent processes.

Received 29 May 2010, accepted 20 July 2010, first published online 24 August 2010

Key words: Europa, Hubble, satellites, spectroscopy.

Introduction

Europa is perhaps the most exciting astrobiological target in the Solar System and an extremely high priority target for Solar System exploration. While Mars may have hosted liquid water oceans in the geological past, it is likely that Europa has a saline liquid water ocean at the present time (Kivelson *et al*. 2000). Europa may therefore be able to sustain life. It is thought that transport may occur between the interior ocean and the surface, from terrain features most reasonably explained by sub-ice-shell activity and the geological youth of the surface (e.g. Figueredo & Greeley 2003, 2004). Interestingly, though a major component of the non-ice material on Europa's surface is almost certainly a hydrated sulfate (Carlson *et al*. 1999; McCord *et al*. 1999), Dalton *et al*. (2003) showed that alternative explanations – some of which pertain to biochemistry – are possible.

In addition to a fascinating solid surface morphology, Europa possesses a tenuous atmosphere and, because of its location deep within the Jovian magnetosphere, auroral activity from the interaction of high-energy particles with the thin gases around the satellite (McGrath *et al*. 2004).

As Europa transitions from sunlight into eclipse, it moves from an environment where harsh, unfiltered ultraviolet (UV) radiation from the Sun is removed, but a high-dosage energetic particle radiation flux onto the surface remains. The absence of sunlight during the eclipse allows us to seek faint intrinsic emission processes induced by this intense particle radiation. In principle, the emission may arise from the extensive swaths of dark reddish material, the highly reflective ices that cover much of the surface and from the tenuous atmosphere and its associated aurora.

Hence, by observing Europa in eclipse, we probe intrinsic emission processes in the atmosphere of Europa and

Table 1. *Observing log for HST Europa observations*

Target	Camera/program visit number	Filters	Exposure times (sec)	Start (date, universal time)
Europa	WFPC2 visit 1	F255W, F300W, F380W, F555W, F675W, F814W, F631N, F656N	500, 10.0, 1.2, 0.11, 0.11, 0.2, 5.0, 8.0	20 March 2007 17:56:18
Europa	ACS/SBC visit 5	PR130L	2600	18 April 2007 04:24:45
Europa-eclipse	WFPC2 visit 2	F300W, F380W, F555W, F675W, F814W	400, 400, 300, 260, 400	14 April 2007 17:18:16
Europa-eclipse	WFPC2 visit 3	F380W, F606W, F814W	600, 600, 600	13 March 2007 18:06:32
Europa-eclipse	WFPC2 visit 4	F656N, F675W, F631N	800, 320, 800	9 May 2007 13:40:04
Europa-eclipse	WFPC2 visit 7	F300W, F380W, F555W, F675W, F814W	600, 400, 300, 260, 400	28 April 2007 21:50:52
Europa-eclipse	ACS/SBC visit 6	PR130L	2600	18 April 2007 06:01:45

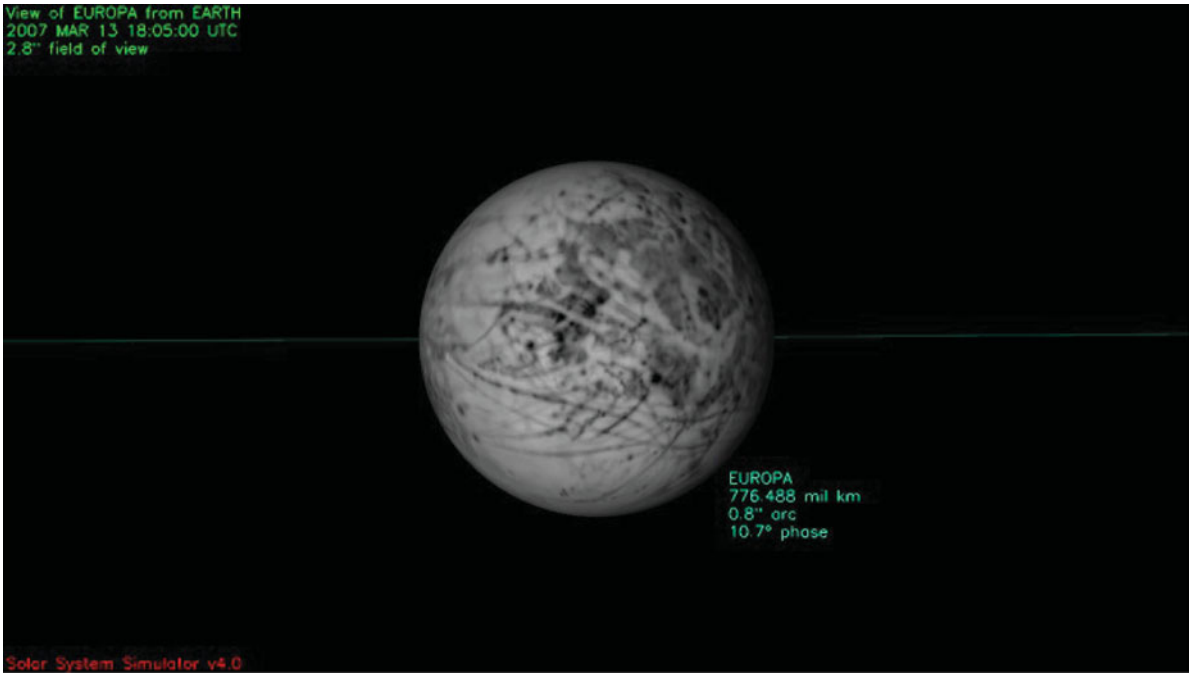

Fig. 1. The configuration of Europa at the time of observations. All data were obtained with Europa at or close to this viewpoint, from http://space.jpl.nasa.gov/. The perspective shows Europa's trailing hemisphere, distinguished by the dark terrain, and a partial view of Europa's sub-Jovian (i.e. Jupiter facing) hemisphere. North is up, East to the left.

potentially also from its surface, which offers the promise of new insights into the environment and physical processes at work on Europa. In particular, if material of biological origin is present, then fluorescent emission would be expected and would offer an excellent diagnostic vehicle. In addition, the interaction between ice and high-energy particles in the form of Cerenkov radiation could be used as a diagnostic of the particle mass and energy distribution and the physical properties of the ice. The amount of Cerenkov radiation escaping the ice will depend on the radiation beam pattern, the particle impact distribution angle and the subsequent scattering in the ice.

Observations and data analysis procedures

Europa was observed in eclipse and out of eclipse for reference under the auspices of The Hubble Space Telescope (HST) Cycle 17 General Observer proposal GO-11861 (P.I. Sparks). Table 1 provides an observing summary. The apparent diameter of Europa over the period of these observations, from

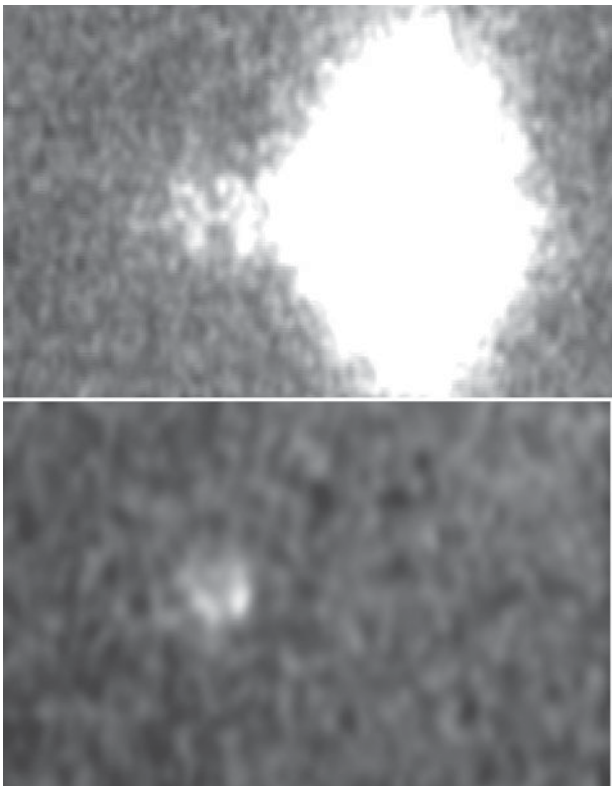

Fig. 2. SBC prism spectra of Europa showing oxygen line emissions at 1304 Å and 1356 Å out of eclipse (upper) and eclipsed (lower). The bright blob of emission in the upper image is the so-called SBC redleak image. North is to the right. The spectrum in sunlight shows two line emission images of Europa at the expected locations of 1304 Å and 1356 Å OI emission, both with the northern limb strongly edge brightened.

20 March 2007 to 9 May 2007, was between 0.83 and 0.97 arcsec. The geodetic longitude and latitude of the centre of Europa changed little for all observations, with longitude ranging from 340 to 352 deg, and latitude −2.8 deg throughout. The out-of-eclipse observations were close to longitude 340 deg, while the in-eclipse observations were all within 1.5 deg of 351 deg, derived using the JPL Horizons system (Giorgini *et al*. 1996). Hence, we are viewing the trailing side of Europa, with a substantial coverage of darker reddish material, as shown in Fig. 1.

The program used the Advanced Camera for Surveys Solar Blind Channel (ACS/SBC) to obtain far ultraviolet (FUV) images with the slitless PR130L FUV prism. These FUV spectra (which exclude geocoronal Lyman α) were taken one orbit each both inside and out of the eclipse. They capture resolved individual monochromatic OI 1356 Å and OI 1304 Å images of Europa. Data in the optical region of the spectrum were obtained using the Wide-Field and Planetary Camera-2 (WFPC2), using a variety of filters designed to probe different aspects of potential optical emission. Data were obtained for all observing configurations outside of eclipse, in sunlight, to provide an empirical reference basis, and a series of full umbral eclipses were observed in four additional visits with different filter combinations. Broad, medium and narrow bandwidth filters were used in the optical and the low-resolution prism for the FUV work.

The FUV data were re-reduced to co-add the two separate spectra, taking proper account of the target motion during the observation. Otherwise, standard reductions were adopted for these data. The SBC in fact is not completely blind to Solar emission and a certain amount of 'redleak' photons is detected. These are apparent in the out-of-eclipse prism observation of Europa, Fig. 2, with an essentially undispersed relatively bright image of Europa at the long wavelength end of the spectrum.

All WFPC2 data were processed through the standard HST calibration pipeline to debias and flat-field the images. Since the WFPC2 has four independent charge-coupled devices (CCDs), we reprocessed the WFPC2 images using the *pyraf* task *multidrizzle*, which combines all images from a single exposure into a single, geometrically rectified output image. We then extracted a region of interest, essentially the field of view of the 'Planetary Camera' (PC) chip, which contained the expected location of Europa at the time of observation. For all observations, the target location was in the corner of the PC chip, close to the apex of the pyramid (which is used to direct the focal plane segments to the separate cameras). The image of Jupiter always lies in the CCD 'opposite' the PC across the pyramid apex; multiple images using the same filter were combined to yield the integration times and filter combinations listed in Table 1.

There is a tremendous amount of light scattered into the field of view from the sunlit face of Jupiter itself, which by necessity is only a few arcseconds from Europa during eclipse observations. To remove the large-scale scattering structures, we devised a special-purpose filtering scheme. Firstly, an eighth order polynomial was fitted to each row and each column separately in every image. The average of the two model images was subtracted from the original data. The fitting algorithm minimized the sum of the absolute deviations from the polynomial, a procedure that is robust against outliers. This processing resulted in a diagonal crisscross pattern of residual scattered light, much reduced in intensity from the original image, hence a second phase of polynomial modelling was used, which fitted quadratics by minimizing the squared residuals to the light distribution along diagonals. Figure 3 illustrates the image processing stages. To test the effect of the low-order filtering on the target, we also applied the same methods to the out-of-eclipse images, expecting a relatively minor loss of flux since Europa is of high spatial frequency compared to the fitting functions. The loss of flux on target was determined to be approximately 17%, which was allowed for in the presentation of flux ratios (Tables 2 and 3).

Since Europa itself is not readily visible in eclipse, for those observations without additional objects in the field, we rely on the default HST pointing, which has a root mean square (RMS) positional uncertainty of approximately 1 arcsec (at the time moving target observations still used the GSC-1 guide star catalogue, with its relatively large absolute positional uncertainty dominating the pointing uncertainty). Where there are additional objects in the field, we attempted

Table 2. *Measured count rate in eclipse relative to sunlit Europa, correcting for small distance dependencies, large 3.0 arcsec aperture*

Filter	Sunlit count rate	Sunlit flux F_λ (erg/s/cm²/Å)	Visit 2 ratio	Visit 3 ratio	Visit 4 ratio	Visit 7 ratio
F255W	243	2.7e-13				
F300W	1.6e4	1.9e-12				6.8e-5
F380W	1.1e5	5.6e-12	1.6e-5	1.9e-5		−3.1e-5
F555W	2.1e6	1.4e-11	−4.4e-6			−1.6e-5
F675W	2.3e6	1.3e-11	−1.7e-5		−2.3e-5	−1.2e-5
F631N	7.3e4	1.3e-11			−3.7e-4	
F656N	4.2e4	1.2e-11			3.7e-5	
F814W	2.0e6	9.9e-12	−5.3e-5	−4.7e-5		−2.6e-5

Table 3. *Measured count rate in eclipse relative to sunlit Europa, correcting for small distance dependencies, 1.5 × Europa diameter aperture*

Filter	Sunlit count rate	Sunlit flux F_λ (erg/s/cm²/Å)	Visit 2 ratio	Visit 3 ratio	Visit 4 ratio	Visit 7 ratio
F255W	243	2.7e-13				
F300W	1.6e4	1.9e-12				1.0e-5
F380W	1.1e5	5.6e-12	2.0e-6	1.3e-5		−4.9e-6
F555W	2.1e6	1.4e-11	1.9e-6			−1.9e-6
F675W	2.3e6	1.3e-11	−3.0e-6		−3.2e-6	−3.7e-6
F631N	7.3e4	1.3e-11			−2.0e-4	
F656N	4.2e4	1.2e-11			3.5e-5	
F814W	2.0e6	9.9e-12	−1.1e-5	−1.4e-4		−4.0e-6

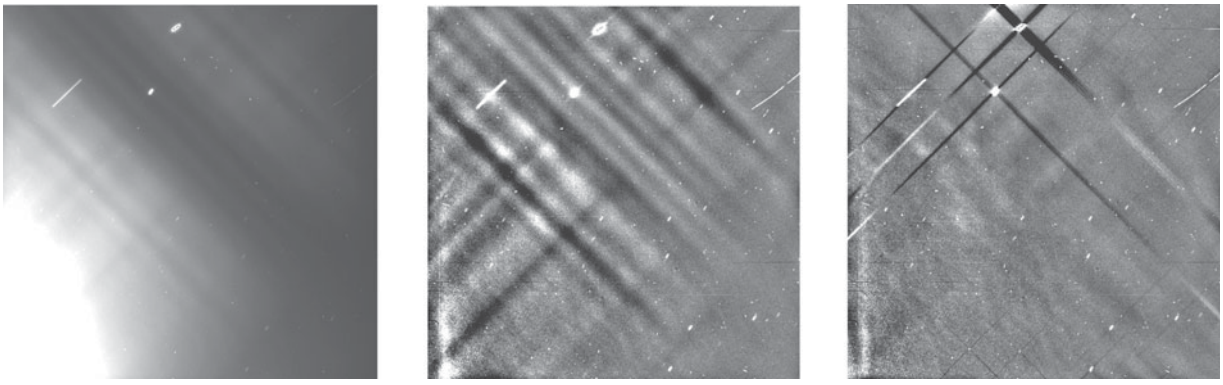

Fig. 3. Successive stages in the removal of scattered light. The first image shows the original data, with an intensity scaling (black to white) 20 times higher than the subsequent two (i.e. 'white' is 20 times brighter in the first image relative to the others). The second shows the effect of removing an eighth-order polynomial fitted to rows and columns and the final image shows a subsequent removal of a quadratic fit to diagonals.

to improve the astrometry of the images (done for visits 1 (which was sunlit as a check), 3 and 7). We present flux levels in Table 2 derived using a large aperture that will include Europa, even if guide star uncertainties are present (we use an aperture diameter 3.0 arcsec which is 3× the RMS pointing uncertainty or a radius of 3.2× that of Europa). A local background sky was estimated for the three sub-image quadrants external to this radius, furthest from the pyramid apex. Table 3 uses a more compact aperture 1.5× the diameter of Europa, which typically reduces the upper limit with the caveat of the presence of pointing uncertainties that may misplace Europa in the measurement aperture. We consider Table 2 to be the most reliable set of limits. Figures 3–5 show the optical image data. There are irregularities in the background that may or may not be emissions, for example in visit 2, filters F555W and F675W (Fig. 5), but they are not statistically significant. Formally, we find upper limits for all eclipse observations, with typical levels of order 10^{-5} times the sunlit brightness. To derive absolute flux values or limits corresponding to the measured count rates, we used the inverse sensitivity and filter width ($\int S d\lambda / S_{\max}$, where S is the system throughput and $S_{\max}$ its maximum value) from the *stsdas/synphot* software, together with the known distance from Horizons Software and assumed isotropic emission. These results are presented relative to an estimate of the total incident power from high-energy ions and electrons in Table 4. (Negative values arise when the measured count rate is less than the surrounding sky, due to statistical noise in the data.)

Discussion

Far ultraviolet spectra: tenous oxygen atmosphere

The recent top prioritization of the Europa Jupiter System Mission for the next outer Solar System flagship mission is focusing attention on the contextual environment of Europa. Surface sputtering by magnetospheric plasma generates a tenuous atmosphere that is dominated by molecular oxygen. FUV emission from this gas is produced by dissociative excitation of the molecular oxygen (Hall *et al.* 1995; Saur *et al.* 1998). In our data, taken with the ACS/SBC, we see this line emission from Europa both in sunlight and eclipse (see Fig. 2). The presence of line emission during eclipse demonstrates that the excitation while in eclipse is due primarily to the local environment of Europa.

We derived a flux level for the intrinsic oxygen line emission during eclipse, which is approximately one half the value

Table 4. *Measurement of optical emission relative to incident radiation energy, given as percent of available energy. For example, 0.05 means a flux of 0.05% of* 3.2×10^{19} *erg* $s^{-1} \approx 1.6 \times 10^{16}$ *erg* s^{-1} (*see text*)

Filter	Sunlit	Visit 2	Visit 3	Visit 4	Visit 7
F255W	28				
F300W	370				0.016
F380W	1053	0.013	0.018		−0.022
F555W	4747	−0.016			−0.53
F675W	3339	−0.04		−0.051	−0.027
F631N	124			−0.03	
F656N	76			0.0018	
F814W	3329	−0.13	−0.14		−0.059

when illuminated by sunlight. The sunlit spectra include a reflected component from the Sun, while the eclipsed emission arises solely from the radiation bombardment and tenuous intrinsic atmosphere of Europa. Utilizing the component level calibration for the ACS/SBC provided by the *synphot* package running under *iraf/stsdas* software, we calculate that the disk average line emission surface brightness in eclipse is 183 Rayleigh, assuming the only eclipse emission is OI where $\lambda = 1356$ Å (or if we assumed an average of 1304 and 1356, then 175 Rayleigh). The disk of Europa in eclipse is dark for the redleak part of the spectrum, corresponding to less than 0.85% of the sunlight illuminated brightness.

While the line emission images of Europa appear to be strongly limb brightened along the northern limb, the absence of a fiducial redleak image in the eclipse image prevents us from establishing a secure zeropoint for the wavelength of the line emission. The strength of the line emission is nevertheless well established at approximately one half that of the sunlit spectrum, indicating significant contributions from both Solar photons and local energetic particle radiation to the presence and excitation of the tenuous atmosphere. In addition, the temperature difference between the eclipsed Europa and sunlit Europa will contribute to the dynamical structure and evolution of the oxygen atmosphere.

Optical images

Figure 4 shows an example of a section of one of the filtered images, with the Jovian ring in the field of view. It is difficult to observe this feature even with the HST, and hence the image serves as a demonstration of the effectiveness of the filtering methods. Figure 5 summarizes the eclipse and out-of-eclipse image data, with the sunlit Europa on the left, and Io on the right from visit 1, with the optical eclipse images from visits 2–4 and 7 in between. The filter sequence goes from top to bottom as described in the caption. Each image section is a 3 arcsec square, with north diagonally to the upper left (40 deg from 'up'). Using our best estimates of the location of Europa, these image sections are centred at the location of Europa. The bright rim on the eastern (left) edge of Europa, particularly in the bluer images, is the region of the moon where the surface is dominated by high albedo ice, rather than the redder material of the trailing hemisphere. Io also shows details on its surface with bright knots and dark patches, particularly in the blue images, which are related to the active volcanism on its surface.

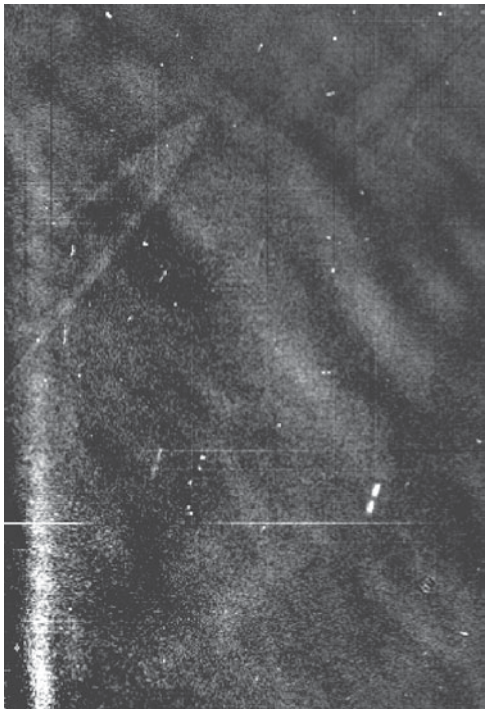

Fig. 4. F675W eclipse image, visit 4, showing Jupiter's main ring above the expected location of Europa which is near the bottom of the image.

Fluorescence occurs in a multitude of solid states in response to high-energy particle radiation, which is intense at the Europan surface. Examples of luminescence include interstellar dust, possibly associated with polycyclic aromatic hydrocarbons (Simonia 2004; Vijh & Witt 2004; Witt & Vijh 2004), cometary materials (Churyumov & Kleshchonok 1999) and laboratory mixes of ices (Grossweiner *et al.* 1954; Quickenden *et al.* 1982), while complex biological molecules abound in fluorescent phenomena. The high-energy particle environment of the Jovian magnetosphere is also likely to produce Cerenkov radiation in the water ice of the Europan surface. Cerenkov emission occurs if the particle speed exceeds light-speed, $v > c/n$, where n is the refractive index. For electrons, this translates to $E > (0.1\ \text{MeV})(1.6/n)^2$. Inspection of Fig. 20.3 in Johnson *et al.* (2004) shows that electrons with energies above such a threshold are a very significant fraction of the total energy flux at Europa. In laboratory simulations of the Europan environment (pure ice, 100 K, 10^{-9} Torr), naked-eye fluorescence of electron irradiated ice can be seen.

The total flux of radiation energy incident on the surface of Europa, from Table 20.3 of Johnson *et al.* (2004), is $5\text{–}8 \times 10^{10}$ keV $\text{cm}^{-2}\ \text{s}^{-1}$, which corresponds to a total energy of $\approx 3.2 \times 10^{19}$ erg s^{-1}. For each of our observations, we calculated the isotropic radiated flux corresponding to the measured countrate and distance of Europa at the time of observation, and present this relative to the total available

Fig. 5. Left, Europa in sunlight, right Io in sunlight, visit 1. Between, columns are Europa eclipse images (left to right visits 2–4 and 7) and filters top to bottom F255W, F300W, F380W, F555W, F675W, F631N, F656N, F814W, with stray light removed as far as possible through data processing. Typical brightnesses are $\sim 10^{-5}$ those of the sunlit Europa. The orientation is such that north points 40 degrees counterclockwise from the *y*-axis, i.e. close to diagonally lower right to top left. (The central image for visit 3 uses F606W rather than F675W, but is saturated over half the field of the subimage shown and hence is not used.)

energy from energetic ions and electrons, assuming an incident flux of $5–8 \times 10^{10}$ keV cm^{-2} s^{-1}. Any radiation-induced emission is likely to be more isotropic than the highly anisotropic illumination by the Sun, although it is thought that there is a preferential distribution of incident particles on the trailing side of Europa, which we are observing. Table 4 shows that the upper limits typically are of order of 0.5% to 0.05% of the available incident energy in any one filter. Quickenden *et al*. (1982) calculated the luminescence yield to be $2.4 \pm 0.6 \times 10^{-6}$ photons/eV for high purity ice at 88 K irradiated by a pulsed 0.5 MeV electron beam. Importantly, this emission is confined to a relatively narrow optical band (Freeman *et al*. 1984). Our upper limit for the yield, derived from HST results for Europa in eclipse, is about an order of magnitude greater than that of Quickenden *et al*. (1982).

Conclusions

We have shown that the FUV OI line emission from the tenuous oxygen atmosphere of Europa can be detected both in eclipse and out of eclipse. Out of eclipse, the oxygen line emission is strongly anisotropic in its distribution, with limb-brightened emission around the northern limb of Europa. The emission strength remains at about one half the sunlit strength during the eclipse. This clearly demonstrates that the high-energy radiation particle environment of Europa is contributing significantly to the presence and excitation of the oxygen atmosphere, although a number of effects will lead to structural differences in the two sets of conditions. During the Cassini flyby of Jupiter, Porco *et al*. (2003) observed Europa during eclipse in white light and detected optical emission and observed some patches and limb brightening. They attribute the optical emission to a mix of illumination by Ganymede and intrinsic atmospheric emission. We have not detected any statistically significant optical emission when Europa is in the shadow of Jupiter. Energetically, the flux limits typically correspond to 0.01% to 0.5% of the available total energy from incident particles, and since Europa may have additionally been illuminated by light refracted through Jupiter's upper atmosphere and light scattered from the other Galilean satellites, the flux limits for induced radiation are likely to be smaller than our measured upper limits. Nevertheless, Cerenkov emission must be present, and with more sensitive observations and better knowledge of the emission wavelength and beam pattern of Cerenkov emission in ice, it may yet prove feasible to detect it using HST observations. Beyond Cerenkov emission, our limits on global fluorescent emission induced by energetic particles suggest that this is not a strong component in Europa. If it were to prove feasible using deeper observations, or observations that are less sensitive to scattered light, then an important new suite of diagnostic tools would be available for the characterization of Europa and its environment.

Acknowledgements

This work was based on observations with the National Aeronautics and Space Administration (NASA)/European Space Agency (ESA) HST, which is operated by the Association of Universities for Research in Astronomy, Inc., under NASA contract NAS5-26555.

Support for this work was provided by NASA through grant GO-11085 from the Space Telescope Science Institute, which is also operated by the Association of Universities for Research in Astronomy, Inc., under NASA contract NAS5-26555.

References

Carlson, R.W., Johnson, R.E. & Anderson, M.S. (1999). *Science* **286**, 97.

Churyumov, K.I. & Kleshchonok, V.V. (1999). *American Astronomical Society, Division of Planetary Science Abstracts* **31**, 1713.

Dalton, J.B., Mogul, R., Kagawa, H.K., Chan, S.L. & Jamieson, C.S. (2003). *Astrobiology* **3**, 505.

Figueredo, P.H. & Greeley, R. (2003). *Astrobiology* **3**, 851.

Figueredo, P.H. & Greeley, R. (2004). *Icarus* **167**, 287.

Freeman, C.G., Quickenden, T.I., Litjens, R.A.J. & Sangster, D.F. (1984). *J. Chem. Phys.* **81**, 5252.

Giorgini, J.D. *et al*. (1996). *Bull. Am. Astron. Soc.* **28(3)**, 1158 (Horizons).

Grossweiner, L.I. & Matheson, M.S. (1954). *J. Chem. Phys.* **22**, 1514–1526.

Hall, D.T., Strobel, D.F., Feldman, P.D., McGrath, M.A. & Weaver, H.A. (1995). *Nature* **373**, 677.

Johnson, R.E., Carlson, R.W., Cooper, J.F., Paranicas, C., Moore, M.H. & Wong, M.C. (2004). Radiation effects on the surfaces of the Galilean satellites. In *Jupiter: Planet, Satellites, Magnetosphere*, ch. 20, ed. Bagenal, F., Dowling, T. & McKinnon, W. Cambridge University Press, Cambridge.

Kivelson, M.G., Khurana, K.K., Russell, C.T., Volwerk, M., Walker, R.J. & Zimmer, C. (2000). *Science* **289**, 1340.

McCord, T.B. *et al*. (1999). *J. Geophys. Res.* **104**, 11 827.

McGrath, M.A., Lellouch, E., Strobel, D.F., Johnson, R.E. & Feldman, P.D. (2004). Satellite atmospheres. In *Jupiter: Planet, Satellites, Magnetosphere*, ch. 19, ed. Bagenal, F., Dowling, T. & McKinnon, W. Cambridge University Press, Cambridge.

Porco, C.C. *et al*. (2003). *Science* **299**, 1541.

Quickenden, T.L., Trotman, S.M. & Sangster, D.F. (1982). *J. Chem. Phys.* **77**, 3790.

Saur, J., Strobel, D.F. & Neubauer, F.M. (1998). *J. Geophys. Res.* **103**, 19 947.

Simonia, I.A. (2004). *Astrophysics* **47**, 530.

Vijh, U.P. & Witt, A.N. (2004). *Astrophys. J.* **606**, L65.

Witt, A.N. & Vijh, U.P. (2004). In *Proc. Conf. Astrophysics of Dust*, ASP 309, p. 115.